Microsc. Microanal. 11, 1–13, 2005
DOI: 10.1017/S1431927605050087

Microscopy AND Microanalysis

© MICROSCOPY SOCIETY OF AMERICA 2004

Off-Axis Electron Holography of Unbiased and Reverse-Biased Focused Ion Beam Milled Si *p-n* Junctions

Alison C. Twitchett, Rafal E. Dunin-Borkowski,* Robert J. Hallifax, Ronald F. Broom, and Paul A. Midgley

Department of Materials Science and Metallurgy, University of Cambridge, Pembroke Street, Cambridge CB2 3QZ, UK

Abstract: Off-axis electron holography is used to measure electrostatic potential profiles across a silicon *p-n* junction, which has been prepared for examination in the transmission electron microscope (TEM) in two different specimen geometries using focused ion beam (FIB) milling. Results are obtained both from a conventional unbiased FIB-milled sample and using a novel sample geometry that allows a reverse bias to be applied to an FIB-milled sample *in situ* in the TEM. Computer simulations are fitted to the results to assess the effect of TEM specimen preparation on the charge density and the electrostatic potential in the thin sample.

Key words: off-axis electron holography, *p-n* junction, reverse bias, electrostatic potential, electric field, charge density, focused ion beam milling, specimen preparation

Introduction

The ability to characterize ever smaller device features is of great importance for the future development of semiconductor technology. For this reason, the semiconductor industry has demanded a two-dimensional dopant profiling technique that has a spatial resolution of better than 10 nm and a sensitivity to dopant concentration, or alternatively to dopant potential, of better than 10%. Off-axis electron holography in the transmission electron microscope (TEM) has the potential to satisfy these requirements. The technique, which is described in detail elsewhere (e.g., Dunin-Borkowski et al., 2004), can be used to reveal the phase shift ϕ of a high-energy electron wave that has passed through a thin specimen (typically below 0.5 μm in thickness). For a nonmagnetic specimen, in the absence of dynamical diffraction, ϕ can be described by the equation

$$\phi(x, y) = C_E \int V(x, y, z)\, dz \qquad (1)$$

where V is the electrostatic potential (arising from the dopant potential, external electrostatic fringing fields, and the mean inner potential of the specimen), z is a direction parallel to, and x and y are directions perpendicular to, the electron beam, and C_E is a specimen-independent constant that takes a value of 7.3×10^6 rad V^{-1} m^{-1} at a microscope accelerating voltage of 200 kV. If the potential is uniform along z within a specimen of thickness t, then equation (1) can be simplified to

$$\phi(x, y) = C_E V(x, y) t(x, y). \qquad (2)$$

Equations (1) and (2) suggest that electron holography can be used to provide a direct measure of the variation in electrostatic potential in a semiconductor device if a suitable specimen, in which the electrostatic potential is representative of that in the original wafer, can be fabricated. However, it is increasingly recognized that TEM specimen preparation can have a significant influence on the electrical properties of a semiconductor device, both because of physical damage to the specimen surface and because of the implantation of ions such as gallium and argon (McCartney et al., 2002). As a result, it is important to assess the effect of different TEM specimen preparation techniques on dopant potentials measured using electron holography if the technique is to be used to characterize the electrical properties of semiconductor devices with confidence.

Attempts have been made to use TEM-based phase contrast techniques to characterize doped semiconductors since the 1960s (e.g., Titchmarsh et al., 1969; Darlington & Valdré, 1975; Merli et al., 1974, 1975). Theoretical studies were at first used to suggest that phase contrast from *p-n* junctions should be dominated by electrostatic fringing fields *outside* TEM specimens (e.g., Vanzi, 1984). However, Frabboni et al. (1985) used off-axis electron holography to show that a measurable fringing field was only present outside a (chemically thinned) silicon *p-n* junction when it

Received September 22, 2003; accepted April 2, 2004.
**Corresponding author*. E-mail: rafal.db@msm.cam.ac.uk

was reverse-biased *in situ* in the TEM. Recent studies have confirmed this observation for specimens prepared using other techniques, including focused ion beam (FIB) milling (e.g., Twitchett et al., 2002), and have also allowed the clear observation of variations in potential *inside* TEM specimens of semiconductor devices. These studies have revealed that the step in potential measured across an unbiased *p-n* junction is often much lower than the expected built-in voltage across the junction (e.g., Rau et al., 1999; Wang et al., 2002*a*). This discrepancy has generally been explained by introducing the concept of "dead" layers on the specimen surfaces, which are depleted electrically and are usually assumed to have the same thickness on the *p* and *n* sides of the junction. Surprisingly, McCartney et al. (2002) reported that an electrically dead layer was not required to explain results from specimens that had been wedge-polished and subjected to limited argon-ion milling and carbon coating. The difference between these observations is not understood, but is thought to arise from the effects of different TEM specimen preparation techniques on electrostatic potentials in thin, electron-transparent specimens. A separate issue, which is also of considerable importance, relates to the validity of examining "unbiased" TEM specimens of semiconductor devices, some parts of which may be floating electrically, rather than specimens that have electrical contacts applied to their active regions during examination in the TEM (Beleggia et al., 2000).

In this article, which expands on a preliminary study (Twitchett et al., 2002), we address both of these issues by using off-axis electron holography to characterize a silicon device that contains a single *p-n* junction. In this sample, there are no metalization layers or other changes in composition, which could complicate specimen preparation or interpretation of the results. We concentrate on the effect on the measured phase shift of using FIB milling to prepare the thin TEM specimen. This technique is now widely used to prepare site-specific regions of semiconductor devices for TEM examination using electron holography (e.g., Wang et al., 2002*b*; Donnet et al., 2003). However, it is known to result in damage to the surface of the specimen, as well as gallium implantation, preferential thinning ("curtaining"), and dopant deactivation (e.g., Langford & Petford-Long, 2001).

To apply a voltage across an FIB-milled specimen *in situ* in the TEM, we introduce a novel specimen geometry that allows two electrical contacts to be applied to the sample. In addition to the benefit of examining a "working" semiconductor device in the TEM, a second advantage of examining a specimen under an applied electrical bias is that unwanted contributions to the contrast from specimen thickness variations and strain can, in principle, be removed by taking the difference between holographic phase images recorded at different applied voltages.

When interpreting phase profiles measured from both unbiased and biased specimens, we fit empirical computer models to the results to allow the charge density profile and

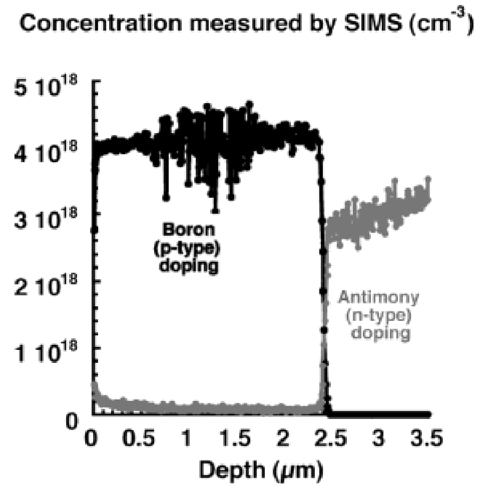

Figure 1. Secondary ion mass spectrometry (SIMS) profile obtained from the specimen examined in this study, which contains a single *p-n* junction at a depth of ~2.5 μm below the wafer surface. The *absolute* concentration of each element in the profile is only estimated to be accurate to ~30%, whereas the relative concentration with depth is thought to be much more reliable (R.L. Hervig, pers. comm.).

the depletion width across the *p-n* junction to be measured quantitatively. The charge density profile is of particular interest as it provides a highly sensitive measure of the effect of specimen preparation on the properties of a semiconductor device. Our measurements allow us to draw conclusions about the effect of FIB milling on the electrostatic potential both within the specimen and on its surfaces, as well as about the degree to which *unbiased* FIB-milled specimens can be used to provide reliable and accurate results about dopant potentials.

Materials and Methods

A silicon *p-n* junction, which comprised a 2.5-μm-thick boron-doped *p*-type layer grown directly onto an antimony-doped *n*-type substrate using molecular beam epitaxy, was prepared for TEM examination in an FEI 200 FIB workstation. The dopant concentration on each side of the junction was in excess of 10^{18} cm^{-3}, as confirmed by the secondary ion mass spectrometry (SIMS) profile shown in Figure 1. Great care was taken during FIB milling to ensure that the focused gallium ions were only directed parallel to the surfaces of the thin membrane. In this way, gallium implantation was minimized, although not excluded completely. The current of the gallium beam used to form the final membrane was 150 pA, with a probe (full width at half maximum) of 10 nm. In the present study, no further specimen preparation was undertaken before examination in the TEM.

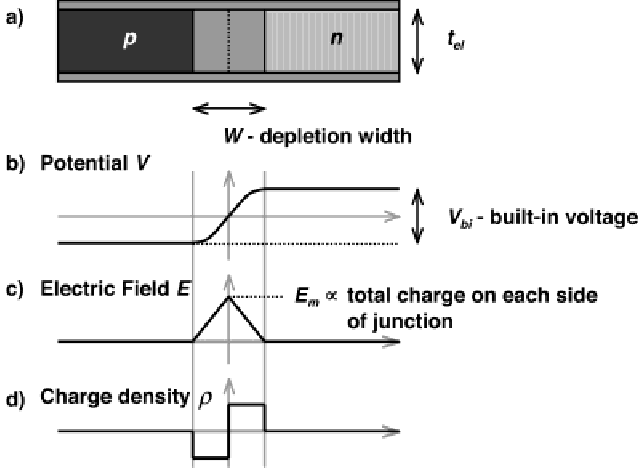

Figure 2. a: Schematic diagram showing the cross-sectional geometry of a TEM specimen that contains a *p-n* junction. t_{el} is the "electrically active" specimen thickness. The shaded areas at the top and bottom surfaces of the specimen represent electrically passivated (or depleted) layers, whose physical and electrical nature are affected by TEM specimen preparation. **b–d:** Schematic diagrams of the electrostatic potential, electric field, and charge density profiles, respectively, across an abrupt, symmetrical *p-n* junction. V_{bi} is the built-in voltage, and W is the width of the depletion region over which the potential changes. The sign convention for the potential is consistent with the mean inner potential of the specimen being positive relative to vacuum.

The predicted electrostatic potential $V(x)$, electric field $E(x) = -dV/dx$ and charge density $\rho(x)$ across a *p-n* junction are related to each other by Poisson's equation

$$\frac{d^2V(x)}{dx^2} = -\frac{\rho(x)}{\varepsilon_r \varepsilon_0} \tag{3}$$

where ε_r is the relative permittivity of the semiconductor and ε_0 is the permittivity of free space. The basic form that these three profiles would be expected to take for an abrupt *p-n* junction are shown schematically in Figure 2 (Sze, 2002). These graphs are drawn on the assumption that the "transition regions" on each side of the depletion region are negligibly small—an assumption that is unlikely to be true in practice, but which can be assessed experimentally by calculating the charge density profile from a measured phase profile (see below).

In Figure 2, the effect of the unknown electrical state of the specimen surface on the potential is modeled phenomenologically by assuming the presence of an electrically dead layer of uniform thickness on the specimen surfaces. The true junction potential is then assumed to lie within thickness t_{el}, which is smaller than the total specimen thickness t. It should be noted that care is required both with specimen preparation and with interpretation of measured phase shifts because the mean inner potential of silicon is approximately 12 V, and as a result a small change in specimen thickness (of 5–10%) can result in similar contrast to that across a *p-n* junction.

Standard FIB milling (e.g., Langford & Petford-Long, 2001) was used to prepare membranes of six different thicknesses within two adjacent "windows" (referred to as Windows A and B below) on a single TEM specimen. In addition, a new specimen geometry, which is illustrated in Figure 3a,b, was developed to examine the same *p-n* junction under an applied electrical bias *in situ* in the TEM. The approach involved cleaving a 1–2 mm square of wafer, which had been polished from the substrate side to a thickness of ~50 μm. FIB milling was then carried out on one corner of the square to provide an area of uniform thickness on a specimen that was large enough to handle, but which could also be clamped between two spring contacts to apply a bias across the junction in the TEM. For both the unbiased and the biased sample geometries, the region of interest on the specimen was always protected from gallium implantation and damage by depositing a thin strap of platinum onto the wafer surface before FIB milling.

As a result of the relatively large distance of 2.5 μm between the wafer surface and the junction, additional FIB cuts were needed in all of the membranes, as shown in Figure 3b, to provide a vacuum reference near the *p-n* junction for off-axis electron holography. *In situ* biasing experiments were carried out using a home-built, two-contact biasing holder, which was modified from a conventional Philips heating holder and is shown schematically in Figure 3c. The original substrate side of the cleaved wafer was glued onto the thin straight edge of a semicircle of copper using conducting silver epoxy. This semicircle was then clamped onto a copper track that had been patterned onto a piece of printed circuit board, which had a hole drilled into it for the electron beam to pass through. A second spring contact was then applied to the original front surface of the wafer. Reverse-bias voltages of up to 3 V were applied to the sample during the experiments described below.

Off-axis electron holograms of each *p-n* junction specimen were acquired using a Philips CM300 field emission gun (FEG) TEM equipped with a SuperTwin objective lens and an additional high-strength Lorentz minilens. The technique, which is illustrated in the form of a ray diagram in Figure 4a, involves using an electrostatic biprism (here, a 0.6-μm-diameter quartz wire coated with gold) to overlap an electron wave that has passed through the specimen with a part of the same electron wave that has passed only through vacuum. The resulting interference pattern, or electron hologram, contains interference fringes whose intensity and spacing can be used to measure the local amplitude and phase shift of the electron wave that has passed through the specimen, respectively. Details of the approach used to extract the amplitude and phase shift from a hologram are described elsewhere (e.g., Dunin-Borkowski et al., 2004).

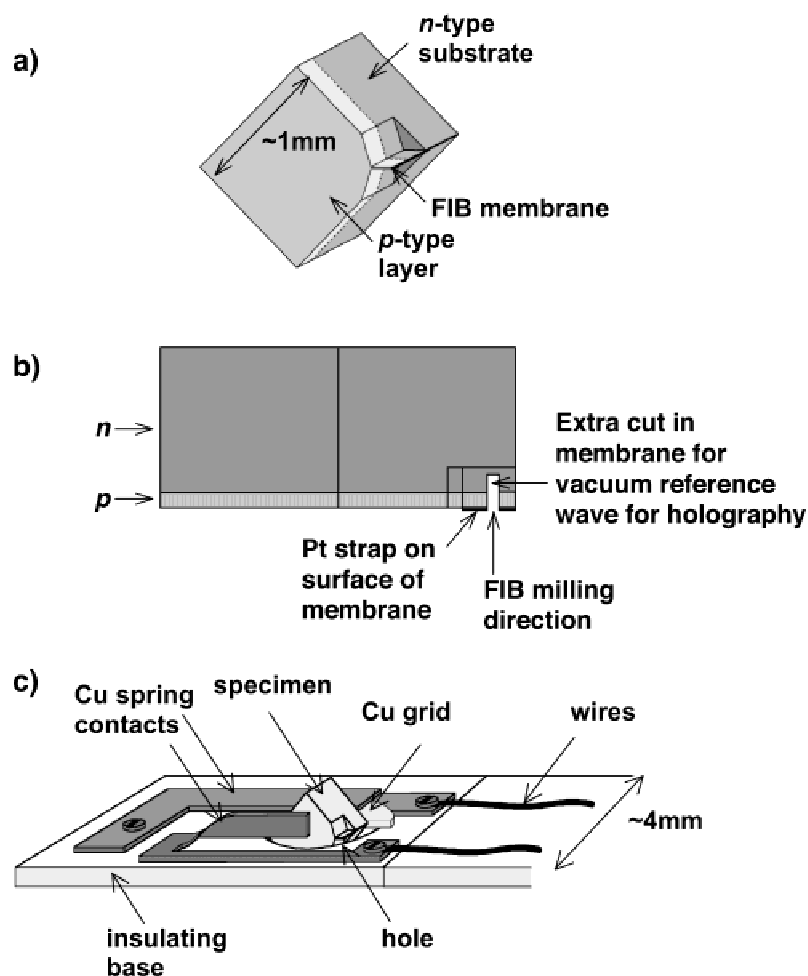

Figure 3. a: Schematic diagram showing the specimen geometry for electrical biasing experiments. The specimen is prepared by cleaving a 1–2 mm square from the Si wafer, one corner of which is subsequently FIB milled parallel to the original wafer growth direction. **b:** Schematic diagram (not to scale) showing the Pt strap used to protect the specimen during FIB milling and the extra cut required for the vacuum reference wave for off-axis electron holography. **c:** Schematic diagram of the end of the home-built electrical biasing TEM specimen holder, with the specimen in place.

For the experiments described below, the microscope was operated at an accelerating voltage of 200 kV (rather than 300 kV) to minimize the effects of knock-on damage on the silicon specimen. The use of a Lorentz lens instead of the conventional microscope objective lens, combined with a further increase in the strength of the diffraction lens, allowed an optimal overlap region of 0.5–0.8 μm to be achieved with a biprism voltage of 70–100 V and an interference fringe spacing of 5–10 nm. Holograms were acquired digitally on a 2048 pixel charge-coupled device (CCD) camera, which was located at the end of a Gatan Imaging Filter (GIF) 2000 (Gatan, Pleasanton, California), using acquisition times of between 4 and 16 s. Additional holograms were acquired from vacuum immediately after each hologram of the specimen to remove geometric distortions and other artifacts associated with the imaging and recording process (de Ruijter & Weiss, 1993). All holographic reconstruction and image processing were carried out using library programs written in the Semper image processing language (Saxton et al., 1979). Specimens were always tilted by 1–2° from the ⟨100⟩ zone axis, while keeping the *p*-*n* junction edge-on to better than 0.2°, to ensure that contributions to the contrast from dynamical diffraction were minimized.

Figure 4b shows a representative electron holographic phase image of the silicon *p*-*n* junction, which was initially evaluated modulo 2π and has been "phase unwrapped" everywhere except at the specimen/vacuum interface, where the specimen thickness changes rapidly. The *p*-type and *n*-type sides of the junction exhibit dark and bright contrast in this image, respectively. A gray band, which is visible along the specimen edge, may be indicative of the presence of a depleted, passivated, or damaged surface layer, which is seen directly in cross section in this image but is thought to run around the entire sample surface. Figure 4c,d shows examples of line profiles across the junction measured directly from the recorded phase images, first for three different unbiased specimens, and second for four reverse-bias voltages applied to a single specimen. Reassuringly, all of the profiles agree qualitatively with the expected variation in potential across the junction shown in Figure 2 and with the variation in phase shift expected with both specimen thickness and reverse-bias voltage from equations (1) and (2).

Equations (1) and (2) highlight the importance of obtaining an accurate measure of the specimen thickness when measuring the built-in voltage across the junction from a phase image. Two measurements of specimen thick-

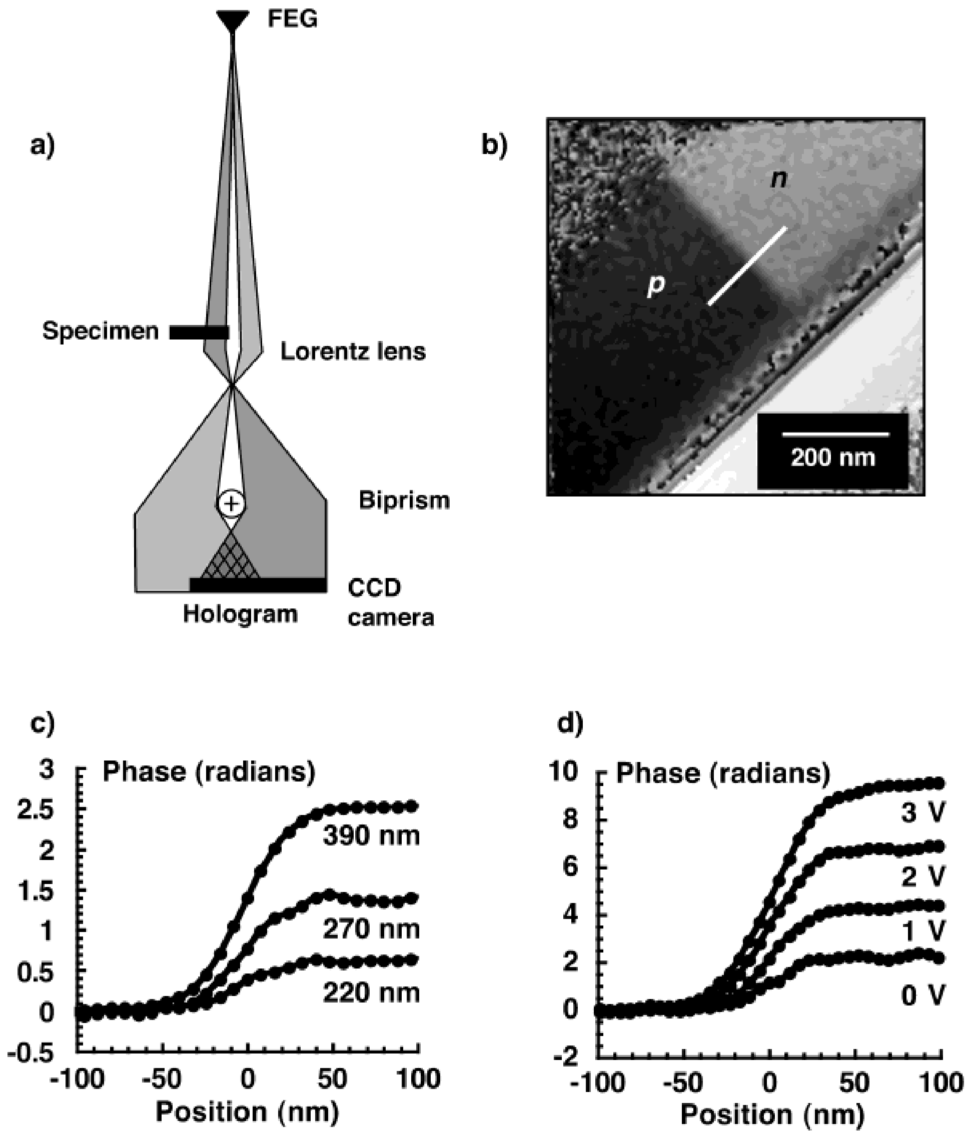

Figure 4. **a:** Schematic diagram showing the electron-optical setup required for off-axis electron holography. The field emission gun (FEG) provides a coherent source of electrons, whereas the Lorentz lens provides an optimal field of view and an optimal holographic interference fringe spacing for acquiring holograms of semiconductor devices. A positive voltage is applied to the biprism wire to form the hologram, which is recorded digitally using a charge-coupled-device (CCD) camera. **b:** Representative phase image reconstructed from an off-axis electron hologram of the Si *p*-*n* junction specimen. No attempt has been made to remove the phase "wraps" at the specimen edge, which is at the lower right of the image. The white line shows the region from which phase profiles were obtained for subsequent analysis. **c:** Experimental phase profiles obtained from three unbiased FIB-milled specimens of crystalline thickness 220, 270, and 390 nm. **d:** Similar phase profiles obtained as a function of reverse-bias voltage from a single FIB-milled specimen whose crystalline thickness was measured to be 390 nm.

ness were therefore obtained from each specimen. First, the crystalline thickness t_{cr} was measured from the spacings of fringes visible in convergent beam electron diffraction (CBED) patterns acquired with the specimen tilted to a $\mathbf{g} = 400$ two-beam condition (Williams & Carter, 1997). The values of t_{cr} measured from the "unbiased" specimens were 220, 270, and 410 nm in Window A, and 330, 440, and 560 nm in Window B. The value of t_{cr} measured for the specimen used for biasing experiments was 390 nm. Second, a measure of the total (crystalline and amorphous) specimen thickness $t(x, y)$ was obtained, in units of inelastic mean free path λ_{in}, from each holographic amplitude image $A(x, y)$ (after normalizing by the amplitude of the reference image) by using the equation

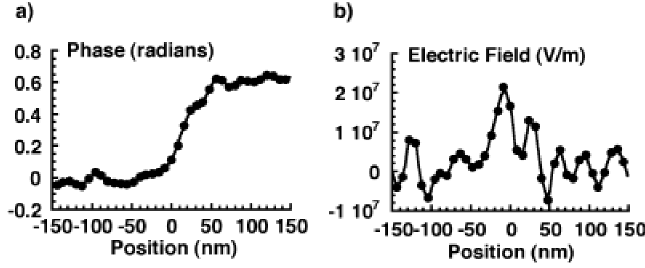

Figure 5. Illustration of the difficulty of determining electric field and charge density profiles directly from a phase profile measured across a *p-n* junction. **a:** A noisy phase profile obtained from an unbiased Si *p-n* junction in a FIB-milled specimen of crystalline thickness 220 nm. **b:** An electric field profile calculated directly from the first differential of the phase profile.

$$\frac{t(x,y)}{\lambda_{in}} = -2 \ln A(x,y) \quad (4)$$

(McCartney & Gajdardziska-Josifovska, 1994). Although the value of λ_{in} obtained using this equation is strictly a weighted average of that in the crystalline region of the sample and in any amorphous overlayers on its surfaces, these values are expected to be similar here as any amorphous layers are likely to be formed from damaged (or oxidized) silicon.

Simulations

Although Poisson's equation (equation (3)) can, in principle, be used to convert a measured phase profile into an electric field or a charge density profile directly, the resulting profiles are often too noisy for this approach to be useful even if the holographic fringe contrast is high and the original phase profiles appear to be smooth. An example of this difficulty is shown in Figure 5, in which a phase profile obtained from a specimen whose crystalline thickness was measured to be 220 nm is shown alongside the electric field profile that would be derived directly from it. The noise in the original profile is amplified at each stage of differentiation, limiting quantitative analysis of the junction properties. As a result of the noise in the experimental phase profiles and the relatively small number of data points across the depletion region, it was decided to fit simulated phase profiles to each experimental phase profile. The best-fitting *simulated* profiles were then differentiated to provide electric field and charge density profiles across the junction. This procedure is necessarily subjective as it relies on a suitable choice of model to use in the simulation. However, the alternative approach of smoothing the experimental data before differentiating introduces artifacts into the electric field and charge density profiles. The use of such computer simulations is particularly important as it provides direct access to the charge density, which, being the most sensitive parameter to the junction properties, provides the best indication of how specimen preparation has affected the electrical properties of the junction.

One-dimensional simulations, which are described in more detail below, were fitted to the experimental phase profiles. The parameters that were used to determine each simulated profile included the built-in voltage across the junction V_{bi}, the electrically active specimen thickness t_{el}, the depletion width W, a smoothing parameter a that described the departure of the junction properties from an abrupt junction model, and the lateral position of the simulated profile. At each iteration, a Simplex algorithm (Press et al., 1989) was used to determine the next set of parameters to compare with the experimental data, as illustrated in Figure 6. A single phase grating was found to be sufficient to model the transmission of the electron wave through the specimen. Microscope parameters were included using a transfer function, and a periodically repeating profile, with a *p-n* and an *n-p* junction back to back, was used in the simulations to avoid wraparound effects. Each simulated phase profile was unwrapped for direct comparison with the experimental data.

As the true, three-dimensional electrostatic potential within the thickness of a TEM specimen is unknown, three different empirical models for the electrostatic potential in the specimen were tested. A least-squares criterion was then used to optimize the fit of each model and to determine which of the models provided the best fit to the data. Wherever possible, analytical expressions were used to describe the potential, electric field, and charge density profiles. Asymmetry of the junction properties was not included in the present fits.

Model 1 assumed a classical, abrupt *p-n* junction, whose properties are unchanged through the electrically active thickness of the specimen, as shown schematically in Figure 2. In contrast, Models 2 and 3 were based on the assumption that the charge density profile, *when projected through the thickness of the specimen*, is smoother than that for an abrupt junction. This situation could arise physically from the presence of transition regions of finite width at the edges of the space charge region (which may result from partial screening of space charge in the depletion region by mobile charge carriers). In addition, they may describe the change in the electrical properties of the semiconductor close to the specimen surfaces. The primary reasons for choosing these models, which are empirical, is that they are both simple and physically reasonable.

In Model 2, the charge density profile $\rho(x)$ across the junction is described by the equation

$$\rho(x) \propto \left(\frac{1}{W^2}\right)\left[\frac{2x}{\sqrt{a_1^2 + x^2}} - \frac{2x - W}{\sqrt{4a_1^2 + (2x-W)^2}} - \frac{2x + W}{\sqrt{4a_1^2 + (2x+W)^2}}\right] \quad (5)$$

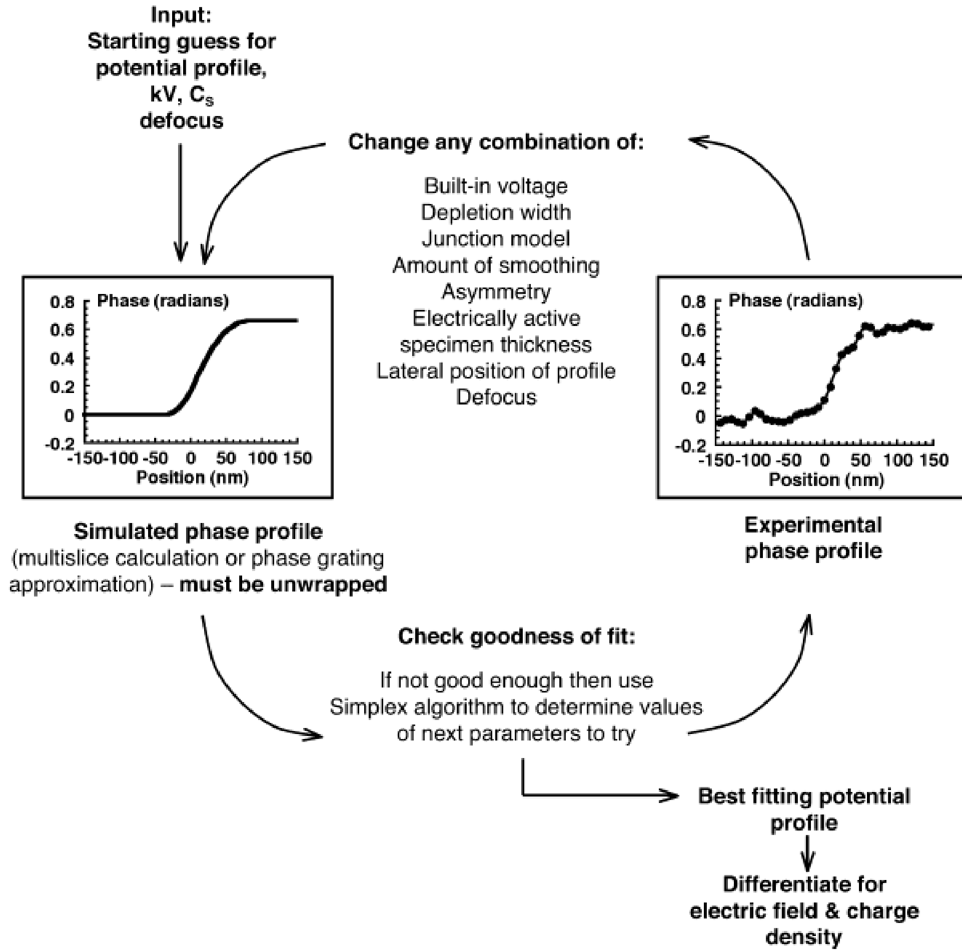

Figure 6. Outline of the fitting procedure used to fit a simulation to an experimental phase profile across a *p-n* junction recorded using off-axis electron holography. The parameters that describe the junction profile in the simulation are selected at each iteration using a Simplex algorithm, and the fit to the experimental data is assessed using the mean of the squared difference between the experimental and simulated profiles.

as shown schematically in Figure 7a for different values of the smoothing parameter a_1, which tends to zero in the limit of an abrupt junction. The equation is normalized so that the total charge on each side of the junction remains constant as W is varied. In Model 3, the charge density profile is assumed to be abrupt (as in Fig. 2) at a given distance from the specimen surface, but the depletion width is allowed to vary through the thickness of the specimen, as shown schematically in Figure 7b. The different curves in the upper image in Figure 7b illustrate the way in which the depletion width is allowed to vary with distance from the specimen surface for different values of the smoothing parameter a_2. This model is suggestive of a higher electrically active dopant concentration in the center of the specimen than close to its surfaces, and perhaps also of an interaction between the surface and junction depletion layers. In Model 3, we describe the depletion width at distance z from the center of a specimen of thickness t by the expression

$$W(z) = W(0) + (a_2 t^3)\left[\frac{1}{(2z+t)^2} + \frac{1}{(2z-t)^2} - \frac{2}{t^2}\right] \quad (6)$$

where $W(0)$ is the depletion width at the center of the specimen (at $z = 0$), the specimen surfaces lie at $z \pm t/2$, and a_2 is again a smoothing parameter that tends to zero in the limit of an abrupt junction.

A final difficulty arises from the fact that, whichever model is used, the built-in voltage and the electrically active specimen thickness can never be determined independently from a *single* phase profile, in which the contrast depends on their product (see equations (1) and (2)). The separation of these parameters is often subjective. Here, it is achieved through a comparison of results obtained as a function of both specimen thickness and applied bias voltage. The assumption that the dead layer thickness is approximately

a) Model 2:
Smoothing function applied to abrupt junction model

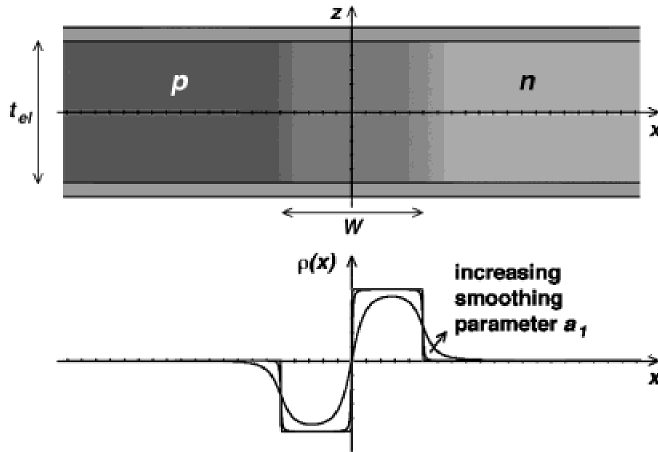

b) Model 3:
Variable depletion width with distance from specimen surfaces

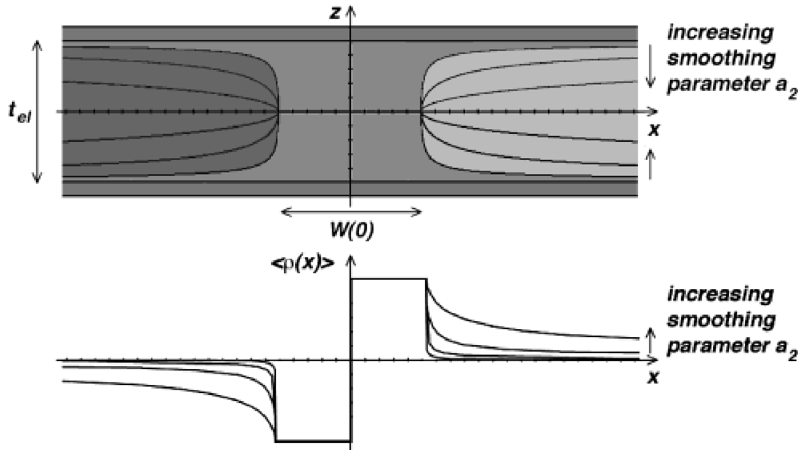

Figure 7. Schematic diagrams showing the empirical models used to generate smoothed *p-n* junction profiles for comparison with experimental phase profiles using the fitting procedure described in Figure 6. Each model allows the transition regions at the edges of the depletion region to have a finite width, and can be used to describe an abrupt junction in the limit of zero smoothing.

independent of these parameters then allows them to be separated (see below).

For comparison with the experimental results, the predicted values of V_{bi} and W for a silicon *p-n* junction are shown as a function of dopant concentration in Figure 8. These graphs are based on the equations

$$V_{bi} = \left(\frac{kT}{e}\right) \ln\left(\frac{N_A N_D}{n_i^2}\right) \tag{7}$$

and

$$W = \sqrt{\left(\frac{2\varepsilon_0 \varepsilon_r}{e}\right)\left(\frac{N_A + N_D}{N_A N_D}\right) V_{bi}} \tag{8}$$

where N_A, N_D, and n_i are the acceptor, donor, and intrinsic concentrations in the silicon device, respectively (Sze, 2002). The graphs in Figure 8 show that for a dopant concentration in excess of 10^{18} cm^{-3} the expected values of V_{bi} and W in an unbiased specimen are ~0.9 V and ~50 nm, respectively.

Experimental Results

Unbiased Specimens

Representative experimental results obtained from the unbiased specimens for the electric field and charge density distributions across the silicon *p-n* junction are shown in Figure 9. These profiles were obtained by fitting Models 2 and 3 to phase profiles similar to those shown in Figure 4c. For each model, the fitted electric field and charge density profiles in Figure 9 are reassuringly consistent, both between the three sample thicknesses shown and between the two models. The results suggest that the *p-n* junction is reasonably abrupt, with 10–20-nm transition regions visible

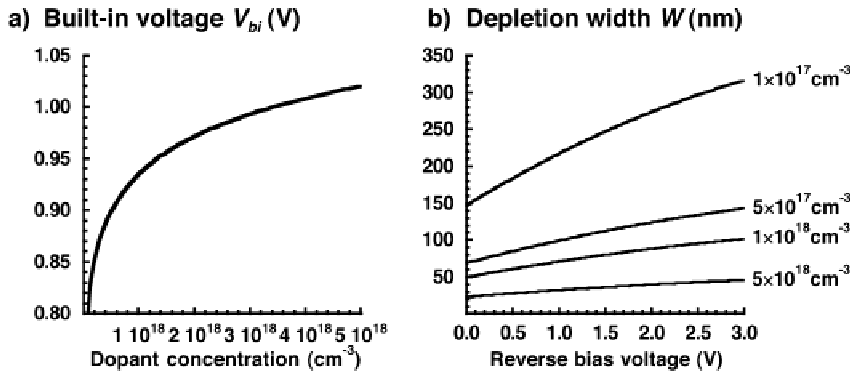

Figure 8. The predicted built-in voltage (**a**) and depletion width (**b**) for a symmetrical, abrupt silicon *p-n* junction at room temperature, plotted for a range of dopant concentrations. Complete dopant ionization is assumed.

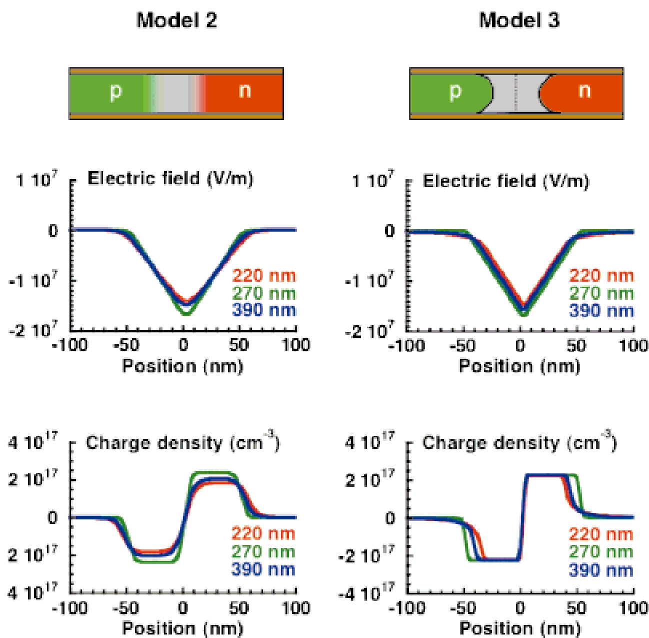

Figure 9. Electric field and charge density profiles derived from best fitting simulations to experimental phase profiles for three unbiased FIB-milled specimens of crystalline thicknesses 220, 270, and 390 nm. The left and right columns show results obtained using two different models for the *p-n* junction potential profile, which are described in the text and in Figure 7. A symmetrical junction was assumed in the simulations.

in the fitted charge density profiles on each side of the depletion region. Model 3, in which the depletion width is assumed to vary with distance from the specimen surfaces, consistently provided a better goodness of fit to the experimental data. However, the difference between the *phase* profiles predicted by the different models was always small, primarily because relatively large changes in the charge density profile across the junction correspond to much smaller differences in the phase.

Despite the qualitative agreement between the experimental profiles shown in Figures 4c and 9 and those expected from Figures 2 and 7, closer inspection of Figure 9 reveals that the fitted charge densities in the depletion region (2–3 $\times$ 10^{17} cm^{-3}) are a factor of 10 lower than expected from the SIMS profiles in Figure 1 ($>10^{18}$ cm^{-3}). The measured depletion widths ($\sim$100 nm) are also consistent with the measured charge densities, and not with the depletion widths predicted from Figure 8 on the basis of the SIMS profile ($<$50 nm). Figure 10 shows the measured depletion width and charge density plotted as a function of the electrically active specimen thickness t_{el} (which was fitted in the simulations on the assumption that V_{bi} = 0.9 V). In these graphs, the depletion width is observed to decrease with increasing specimen thickness. This trend, which would not have been apparent from the phase profiles alone, is indicative of a change in the *projected* depletion width with specimen thickness, and may be associated with the effect on the electrical properties of the junction of the proximity of the specimen surfaces to each other.

The graphs in Figure 10 are plotted as a function of *electrically active* specimen thickness t_{el}, rather than *crystalline* specimen thickness t_{cr}, as the data points obtained from the two different FIB-milled windows on this specimen (A and B) are only then consistent with each other. (Window B has a much greater *crystalline* contribution to the electrically inactive specimen thickness than Window A.) This point is illustrated in a different way in Figure 11, in which the measured phase shifts across the *p-n* junction are plotted as a function of t_{cr}. According to equation (2), these points should all lie on the same straight line, whose intercept with the horizontal axis provides an indication of the crystalline contribution to the electrically dead layer thickness. However, two distinct lines are obtained from Windows A and B, with intercepts close to 100 and 300 nm, respectively. The difference between these results may arise from the exposure of Window B to the gallium beam during FIB milling while Window A was being prepared, at a time when there was no protective platinum deposited over this area. If this interpretation is correct, then it confirms the sensitivity of the crystalline contribution to the electrically dead layer thickness to gallium implantation while also demonstrating the consistency of the results obtained within

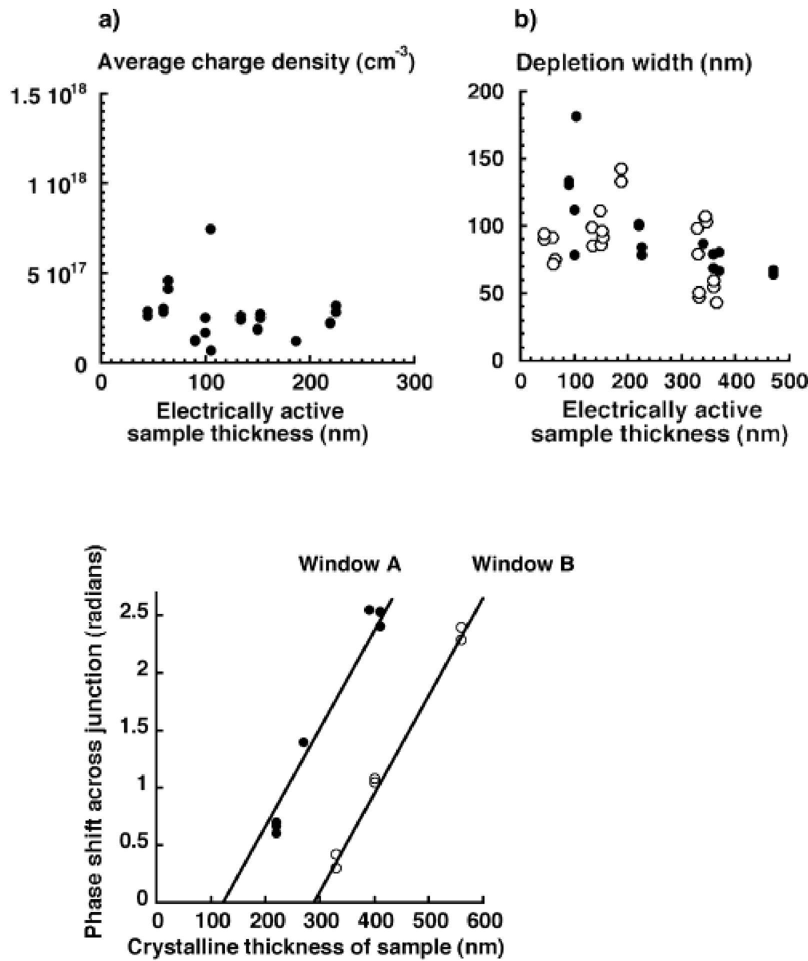

Figure 10. Parameters determined from best fits to experimental phase profiles, plotted as a function of the electrically active specimen thickness, which is inferred from the data on the assumption of a built-in voltage of 0.9 V across the junction. **a:** Average charge density in the depletion region. **b:** Width of depletion region. The solid circles show results obtained after taking great care to ensure that the specimen was FIB milled only at a glancing angle to the surface of the thin membrane (Window A), while the open circles show results obtained from a region of the specimen that is thought to have been implanted with additional gallium (Window B).

Figure 11. The step in phase $\Delta\phi$ across the *p-n* junction examined in this study, measured from off-axis electron holograms of several unbiased specimens of different thickness. The solid circles are obtained from Window A, and show results obtained after taking great care to ensure that the specimen was FIB milled only at a glancing angle to the surface of the thin membrane. The open circles are obtained from Window B, which is thought to have been implanted with additional gallium.

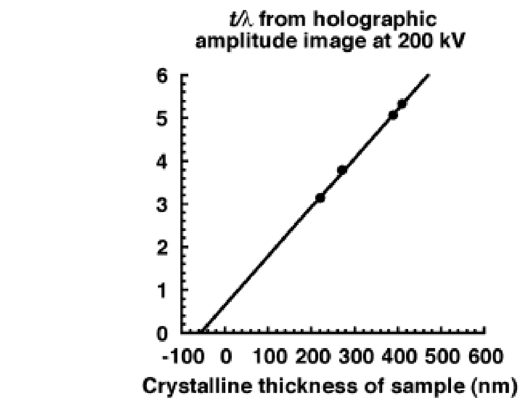

Figure 12. Specimen thickness in units of inelastic mean free path measured from holographic amplitude images and plotted as a function of the crystalline thickness of the specimen measured using convergent beam electron diffraction. The slope of the graph suggests that λ_{in} = 85 nm for silicon at 200 kV (although this value includes contributions to the total inelastic mean free path from amorphous surface layers, in which λ_{in} may be different from that in crystalline silicon). The intercept suggests that 60 nm of the total specimen thickness is amorphous.

the electrically "active" layer of a TEM specimen. An alternative explanation could involve redeposition of material during FIB milling.

Finally, an estimate of the thickness of the (electrically "inactive") amorphous layers on the specimen surfaces can be obtained from Figure 12, which shows a plot of the total specimen thickness, in units of inelastic mean free path, measured from the reconstructed amplitude images as a function of crystalline specimen thickness. The total thickness of the amorphous material is determined to be 50 ± 20 nm from the intercept of the graph with the horizontal axis, suggesting the presence of an amorphous overlayer whose average thickness is 25 ± 10 nm on each surface of the specimen. This amorphous layer could result from damage or sputtering during specimen preparation, from native oxide formation on the exposed silicon surfaces, or from carbon contamination within the microscope.

Reverse-Biased Specimen

Phase images of the *p-n* junction obtained as a function of reverse bias voltage were analyzed in a manner similar to those from the unbiased specimens. These images never revealed detectable fringing fields outside the specimen. This observation is in agreement with the results of Frabboni et al. (1985), and suggests that the surfaces of FIB-milled specimens are always equipotentials, even when subjected to an applied bias. The experimental phase profiles, examples of which were shown in Figure 4d, were matched to simulations using the procedure described in

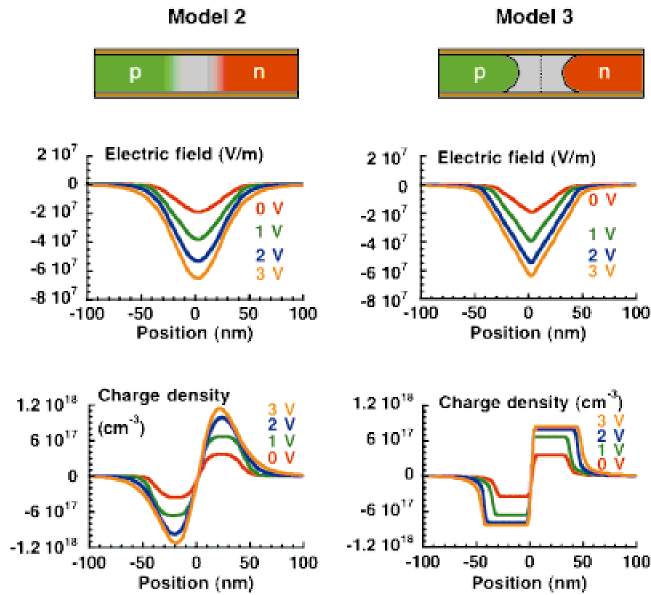

Figure 13. As for Figure 9, but for off-axis data obtained as a function of reverse-bias voltage from a single FIB-milled specimen whose crystalline thickness was measured to be 390 nm.

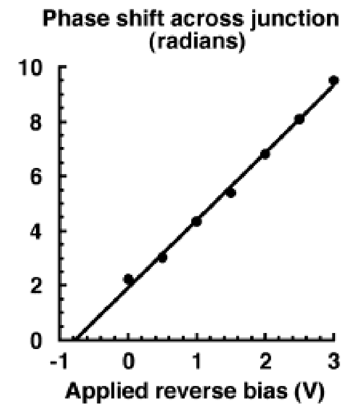

Figure 14. Step in phase $\Delta\phi$ measured across the *p*-*n* junction directly from phase profiles such as those shown in Figure 4d, and plotted as a function of applied reverse-bias voltage. The measurements were obtained from a single specimen whose crystalline thickness was measured to be 390 nm.

Figure 7. The best-fitting electric field and charge density profiles across the junction are shown in Figure 13. Model 3 again consistently provided the best fit to the data.

The fitted charge density profiles in Figure 13 show that the depletion width in the TEM specimen increases with reverse bias voltage, as expected from Figure 8. However, this increase is smaller than expected. The discrepancy is related directly to the fact that the charge density in the depletion region, which is expected to remain unchanged with applied bias voltage, increases with reverse bias from the value measured for an unbiased specimen in Figure 7 to $\sim 10^{18}$ cm^{-3}, a value much closer to that expected for this device. This observation is significant for two reasons. First, it indicates that results obtained from unbiased specimens and from TEM specimens to which electrical contacts (but no voltage) have been applied are consistent with each other. Second, it suggests that some of the dopant that was passivated by specimen preparation has been reactivated simply by applying a bias to the specimen in the TEM. If this observation is correct, then it suggests that *in situ* biasing may be used to remove some of the damage to the electrical properties of semiconductor devices caused by TEM specimen preparation.

Figure 14 shows plots of the phase change across the *p*-*n* junction as a function of applied reverse bias. This graph, together with Figure 13, is important as its linearity and magnitude confirm that the correct potential is always dropped across the *p*-*n* junction. On the assumption that the magnitude of V_{bi} is unchanged with reverse bias, the gradient of the graph in Figure 14, which is given by $C_E \cdot t_{el}$, can be used to infer the electrically active specimen thickness. Similarly, the *x*-axis and *y*-axis intercepts allow a value for the built-in voltage V_{bi} to be determined. The graph provides a measured value for t_{el} of 335 ± 5 nm, suggesting that the electrically dead crystalline layers on each surface of the specimen are 28 ± 5 nm in thickness. The measured value of V_{bi} is 0.9 ± 0.1 V, justifying the use of this value to infer the electrically active specimen thickness above. It should be noted that V_{bi} is far more difficult to measure accurately from the gradients of the graphs shown in Figure 11, as variations in dead layer thickness between different specimens then introduce additional errors.

Discussion and Conclusions

The use of off-axis electron holography to characterize the dopant potential across a silicon *p*-*n* junction, which has been prepared for TEM examination using FIB milling, has been assessed. The internal electrostatic potential profile across the junction has been measured for both a standard FIB geometry and a new geometry that allows *in situ* electrical biasing experiments to be performed in the TEM. The analysis of the results requires a number of assumptions, both because the built-in voltage V_{bi} cannot be separated from the electrically active specimen thickness t_{el} from a single electron hologram and because the difference between the value of t_{el} on the *p* and the *n* sides of the junction is unknown. In the present study, we have assumed that the electrically dead layer thickness is identical on both sides of the junction. The active region of the device is then contained within the central part of the specimen, sandwiched between a crystalline electrically dead layer whose

thickness depends on the amount of gallium implantation and an additional amorphous surface overlayer. We speculate that the crystalline dead layer may result from the presence of point defects, including vacancies and clusters of implanted gallium atoms. *In situ* electrical biasing experiments reveal a built-in voltage across the *p-n* junction of 0.9 ± 0.1 V. For unbiased specimens prepared using FIB milling, results obtained with and without electrical contacts to the active regions of the device are identical to within experimental error.

Our results indicate that, for a simple silicon *p-n* junction, off-axis electron holography can be used to delineate the *position* of the junction. However, a comparison of the measured phase profiles with computer simulations indicates that, within the electrically active part of the specimen, the active dopant concentration is lower than its nominal value as a result of specimen preparation. This effect, which is too large to result solely from the effects of partial degeneracy of the semiconductor or from dopant clustering (Sze, 2002), is not observed when certain other specimen preparation techniques such as small-angle cleaving are used—these results will be presented and discussed elsewhere. Although a technique such as small-angle cleaving provides more quantitative results for the potential, electric field, and charge density across the junction, the assessment and development of FIB milling for electron holographic studies is still essential due to its unparalleled site specificity.

It is most surprising that the electrical activity of the passivated dopant in an FIB-prepared specimen appears to be recovered as a result of *in situ* biasing. Alternative approaches for reactivating the dopant, including limited argon ion milling and low-temperature annealing of the specimen, will also be assessed in future studies. An extensive comparison of both off-axis and in-line holography results with first principles computer simulations of the three-dimensional potential in a TEM sample of arbitrary geometry, with arbitrary surface states and boundary conditions, is also required to allow each of the assumptions described above to be resolved. Such studies, which are in progress both within our research group (Somodi et al., 2003) and elsewhere (Beleggia et al., 2003; Houben et al., 2003), should allow the effect of TEM specimen preparation and electrical biasing on the nature of the surface of the TEM specimen to be understood fully. In-line holograms obtained from the *p-n* junction examined here will be presented elsewhere.

Acknowledgments

We are grateful to Philips Research (Eindhoven) for the Si *p-n* junction specimen, Dr. R. Hervig for the SIMS analysis, and the Royal Society, the EPSRC, and Newnham College, Cambridge, for financial support.

References

Beleggia, M., Cristofori, D., Merli, P.G. & Pozzi, G. (2000). Electron microscopy of reverse biased p-n junctions. *Micron* **31**, 231–236.

Beleggia, M., Fazzini, P.F., Merli, P.G. & Pozzi, G. (2003). Influence of charged oxide layers on TEM imaging of reverse-biased p-n junctions. *Phys Rev B* **67**, 045328.

Darlington, E.H. & Valdré, U. (1975). Imaging of weak Lorentz objects (p-n junctions) by high voltage Fresnel TEM and STEM. *J Phys E* **8**, 321–324.

de Ruijter, W.J. & Weiss, J.K. (1993). Detection limits in quantitative off-axis electron holography. *Ultramicroscopy* **50**, 269–283.

Donnet, D.M., De Veirman, A.E.M., Otterloo, B. & Roberts, H. (2003). Novel FIB-TEM preparation methods for semiconductor device characterisation and failure analysis. *Inst Phys Conf Ser* **180**, 617–620.

Dunin-Borkowski, R.E., McCartney, M.R. & Smith, D.J. (2004). Electron holography of nanostructured materials. In *Encyclopaedia of Nanoscience and Nanotechnology*, Nalwa, H.S. (Ed.), Vol. 3, pp. 41–100. Stevenson Ranch, California: American Scientific Publishers.

Frabboni, S., Matteucci, G., Pozzi, G. & Vanzi, M. (1985). Electron holographic observations of the electrostatic-field associated with thin reverse-biased p-n junctions. *Phys Rev Lett* **55**, 2196–2199.

Houben, L., Luysberg, M. & Brammer, T. (2003). Electron beam illumination effects on electrostatic potential mapping in holographic imaging of semiconductors in transmission electron microscopy. *Inst Phys Conf Ser* **180**, 49–52.

Langford, R.M. & Petford-Long, A.K. (2001). Preparation of transmission electron microscopy cross-section specimens using focused ion beam milling. *J Vac Sci Technol A* **19**, 2186–2193.

McCartney, M.R. & Gajdardziska-Josifovska, M. (1994). Absolute measurement of normalized thickness, t/λ_i, from off-axis electron holography. *Ultramicroscopy* **53**, 283–289.

McCartney, M.R., Gribelyuk, M.A., Li, J., Ronsheim, P., McMurray, J.S. & Smith, D.J. (2002). Quantitative analysis of one-dimensional dopant profile by electron holography. *Appl Phys Lett* **80**, 3213–3215.

Merli, P.G., Missiroli, G.F. & Pozzi, G. (1974). P-n junction observations by interference electron microscopy. *J de Microscopie* **21**, 11–20.

Merli, P.G., Missiroli, G.F. & Pozzi, G. (1975). Electron microscopy observations of p-n junctions. *Phys Stat Sol* (*a*) **30**, 699–711.

Press, W.H., Flannery, B.P., Teukolsky, S.A. & Vetterling, W.T. (1989). *Numerical Recipes*. Cambridge, UK: Cambridge University Press.

Rau, W.D., Schwander, P., Baumann, F.H., Hoppner, W. & Ourmazd, A. (1999). Two-dimensional mapping of the electrostatic potential in transistors by electron holography. *Phys Rev Lett* **82**, 2614–2617.

Saxton, W.O., Pitt, T.J. & Horner, M. (1979). Digital image processing: The Semper system. *Ultramicroscopy* **4**, 343–354.

Somodi, P.K., Dunin-Borkowski, R.E., Twitchett, A.C., Barnes, C.H.W. & Midgley, P.A. (2003). Simulations of the electrostatic potential distribution in a TEM sample of a semiconductor device. *Inst Phys Conf Ser* **180**, 501–504.

Sze, S.M. (2002). *Semiconductor Devices*. New York: Wiley.

Titchmarsh, J.M., Lapworth, A.J. & Booker, G.R. (1969). A new

method for investigating the electric field regions of p-n junctions. *Phys Stat Sol* **34**, K83–K86.

Twitchett, A.C., Dunin-Borkowski, R.E. & Midgley, P.A. (2002). Quantitative electron holography of biased semiconductor devices. *Phys Rev Lett* **88**, 238302.

Vanzi, M. (1984). Theoretical model for studying electrostatic potentials by means of Lorentz microscopy. *Optik* **68**, 319–333.

Wang, Z., Hirayama, T., Sasaki, K., Saka, H. & Kato, N. (2002*a*). Electron holographic characterization of electrostatic potential distributions in a transistor sample fabricated by focused ion beam. *Appl Phys Lett* **80**, 246–248.

Wang, Z., Kato, T., Shibata, N., Hirayama, T., Kato, N., Sasaki, K. & Saka, H. (2002*b*). Characterizing an implanted Si/Si p-n junction with lower doping level by combined electron holography and focused-ion-beam milling. *Appl Phys Lett* **81**, 478–480.

Williams, D.B. & Carter, C.B. (1997). *Transmission Electron Microscopy*. New York: Plenum Press.